Supplementary information for:

Exploring the Effects of Defect Concentrations and Distribution on Li-diffusion in Li_3OBr Solid-State Electrolyte Using the Deep Potential Model

Lirong Xia[a], Jian Tang[b], Yufang Chen[c], Xing Zhou[c], Zhongyun Ma*[a] and Yong Pei* [a,d]

[a]Department of Chemistry, Key Laboratory of Environmentally Friendly Chemistry and Applications of Ministry of Education, Xiangtan University, Xiangtan 411105, P. R. China [b]School of Mathematics and Computational Science, Hunan University of Science and Technology [c]College of Aerospace Science and Engineering, National University of Defense Technology, Changsha 410073, Hunan Province, P. R. China [d] State Key Laboratory of Complex Nonferrous Metal Resources Clean Utilization, Kunming 650093, China

RECEIVED DATE (automatically inserted by publisher)

Corresponding Authors: zhyma@xtu.edu.cn (Z. M.), ypei2@xtu.edu.cn (Y. P.)

1. More details about the DPMD calculations

Accuracy validation of DP models: In order to evaluate the accuracy of the DP model, partial data in the training set and the data for the 3 × 3 × 3 perfect system that is not included in the training set were selected as test set for the error validation of the model. Our test results shows that the average atomic energy error of the DP model for each system is around 10^{-4} eV and the force error is as low as 10^{-3} eV/Å for both the data present in the training set and the data for the 3 × 3 × 3 system. At the same time, the energy and force of the DFT and DP for different systems are plotted in Fig. S2. It is easy to see that the results show a good linear relationship and the R^2 is above 0.99 for both energy and force in each system, which indicates that the trained DP potential function has similar accuracy as the DFT and can be used for subsequent calculations.

Size effect: For MD simulations, the diffusion coefficient is highly dependent on the size of the simulation system, so it is important to consider the effect of different sizes of simulation boxes on the simulation results. Different size of Li_3OBr crystal structures (2×2×2, 3×3×3, 6×6×6, 10×10×10) were thus constructed to obtain simulation boxes containing 40, 135, 1080 and 5000 atoms, respectively, and then the DP model was used to perform the molecular dynamics simulation on these systems under different temperature conditions in order to select an appropriate size for subsequent property analysis. The MSD curves of Li ions at different temperatures for different simulated box sizes are shown in Fig. S2. It can be clearly seen that the fluctuation of the MSD curve gradually decreases with the increase of the simulation size, and when the atoms in the simulation box reach 5000 atoms, the MSD fluctuation is already very small, so the calculation results of this simulation size can be considered as accurate. Therefore, we used a 10×10×10 supercell for subsequent molecular dynamics simulations to study the effects of LiBr-Schottky defects with different concentrations and position distributions on the chemical properties of Li_3OBr materials, and to analyze the dynamic diffusion behavior of Li ions.

In addition, it is worth noting that at 300 K, when the defect concentration is 0.7 %, it is difficult to observe the diffusion behavior of Li ions with 1.2 ns DPMD simulations due to the slow diffusion of Li ions (see Fig. S7a), so we performed 10.2 ns DPMD simulations to observe the diffusion behavior of Li ions under this condition (Fig. S7b).

2. Defect reaction equations

The possible defect reaction equations in Li_3OBr solid-state electrolyte are as follows:

(a) LiBr-Schottky defect:

$$Li_{Li}^{\times} + Br_{Br}^{\times} \rightarrow V_{Li}^{'} + V_{Br}^{\bullet} + LiBr \qquad (S1)$$

(b) LiO_2-Schottky defect:

$$2Li_{Li}^{\times} + O_{O}^{\times} \rightarrow 2V_{Li}^{'} + V_{O}^{\bullet\bullet} + Li_2O \qquad (S2)$$

(c) Br–O anti-sites disorder:

$$Br_{Br}^{\times} + O_{O}^{\times} \rightarrow Br_{O}^{\bullet} + O_{Br}^{'} \quad (S3)$$

Table S1. Defect formation energy of different defects in Li_3OBr.

Defect	μ_i types	μ_i(eV)	$E_{perfect}$(eV)	E_{defect}(eV)	ΔE(eV)
$V_{Li}^{'} + V_{Br}^{\bullet}$	LiBr	-6.63	-166.62	-158.71	1.28
$Br_{O}^{\bullet} + O_{Br}^{'}$	-	-	-166.62	-164.25	2.37
$2V_{Li}^{'} + V_{O}^{\bullet\bullet}$	Li_2O	14.35	-166.62	-150.80	1.47
$V_{Li}^{'}$	Li	1.90	-166.62	-161.18	3.54
$Li_{i}^{\bullet}$	Li	1.90	-166.62	-165.43	3.09
$V_{O}^{\bullet\bullet}$	O_2	9.30	-166.62	-155.39	6.58
$V_{Br}^{\bullet}$	Br_2	1.95	-166.62	-161.17	3.50

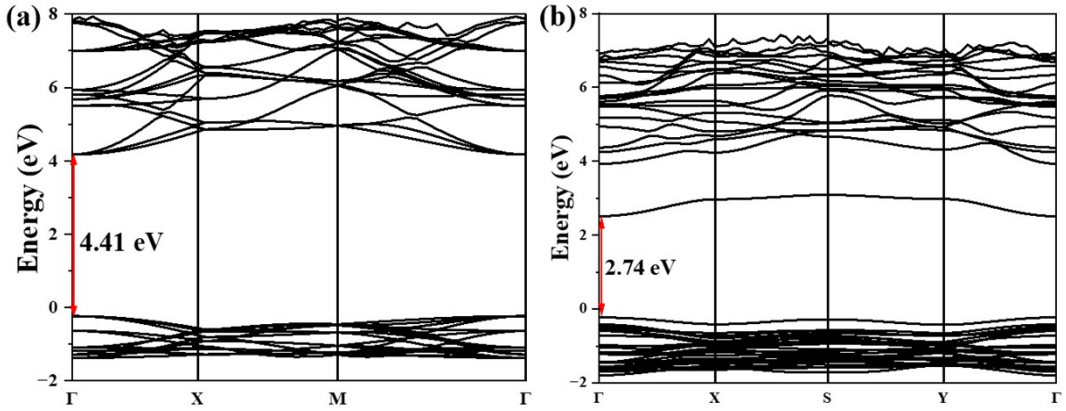

Fig. S1 Band-structure calculated by PBE functional: (a) perfect structure (b) defect structure

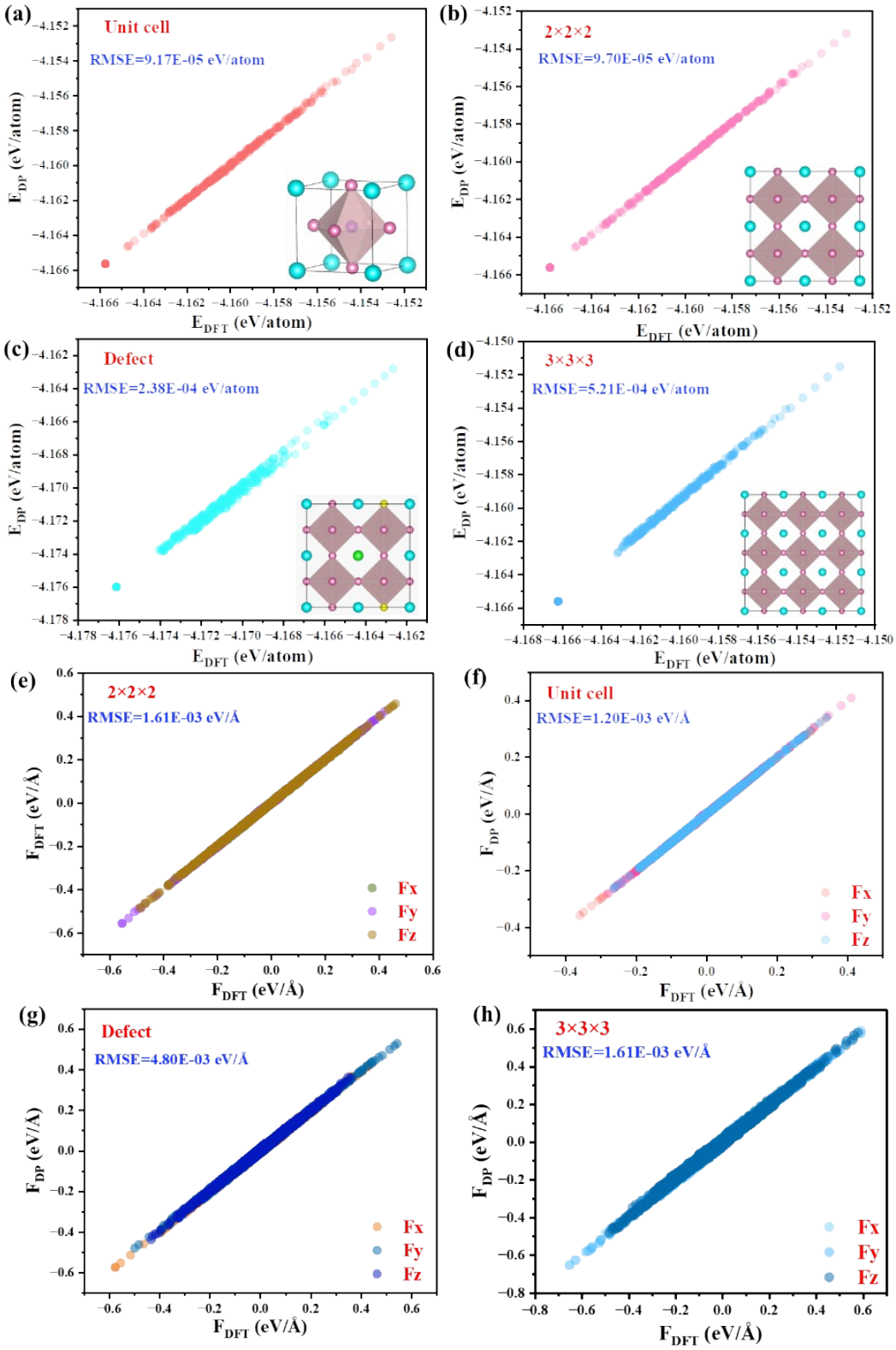

Fig. S2 Comparison of the energy (a-d) and force (e-h) calculated by DFT and DP, respectively.

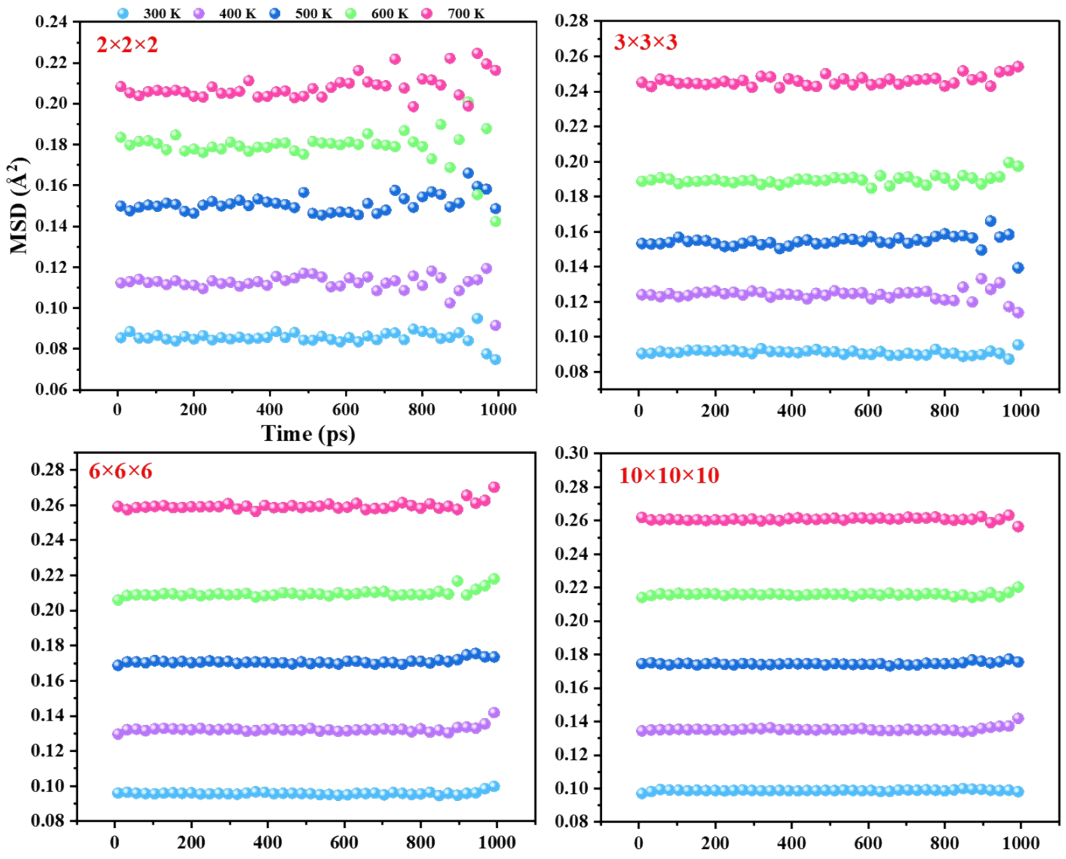

Fig. S3 Li MSD curves of four perfect Li_3OBr crystals with different sizes at 300-700 K.

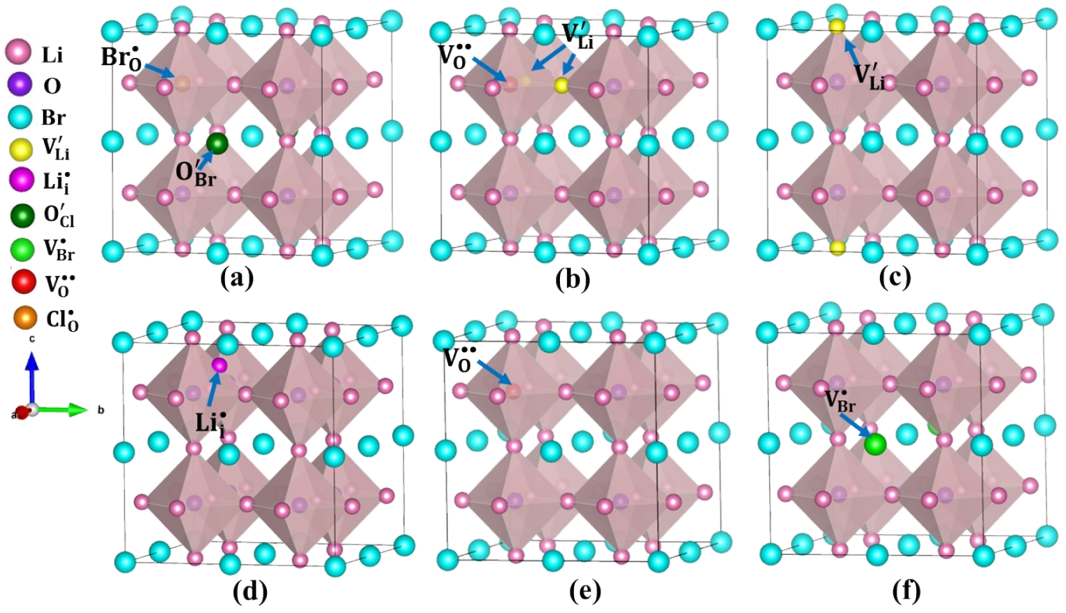

Fig. S4 Schematic diagram of Li_3OBr defective structures: (a) $Br_O^{\bullet} + O_{Br}^{'}$ (b) $2V_{Li}^{'} + V_O^{\bullet\bullet}$ (c) $V_{Li}^{'}$ (d) $Li_i^{\bullet}$ (e) $V_O^{\bullet\bullet}$ (f) $V_{Br}^{\bullet}$

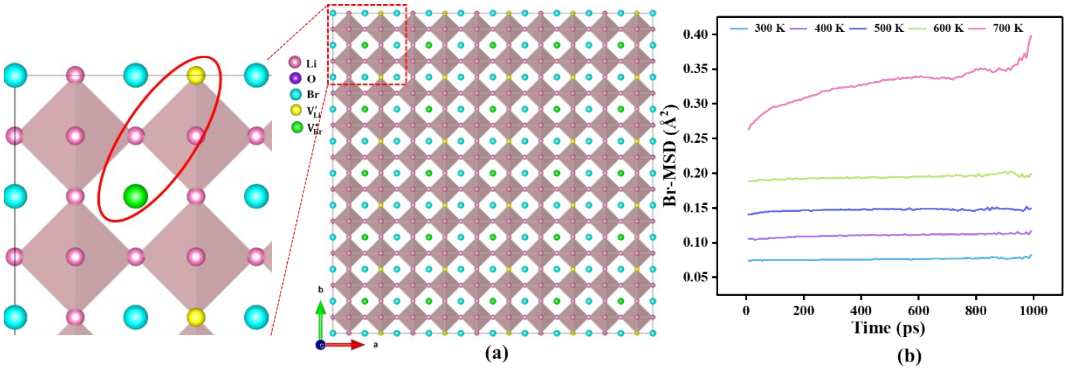

Fig. S5 (a) The structure of Li_3OBr with a defect concentration of 4.2 %. on the left is an enlarged view of the red box with the distribution of Li vacancies and Br vacancies circled in red ellipses. In all concentration ranges, Li vacancies and Br vacancies exist in pairs and are distributed as shown in the elliptical. (b) MSD curves of Br for the system with a defect concentration of 4.2 %.

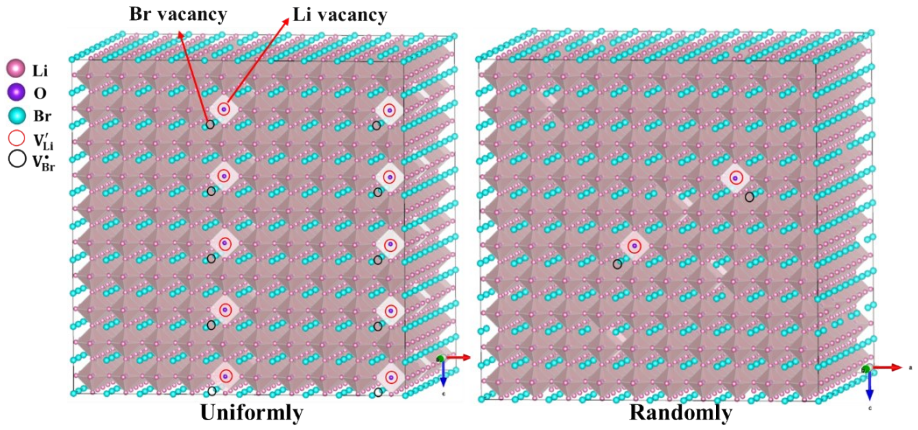

Fig. S6 The structures of Li_3OBr with defects uniformly (a) and randomly (b) distributes.

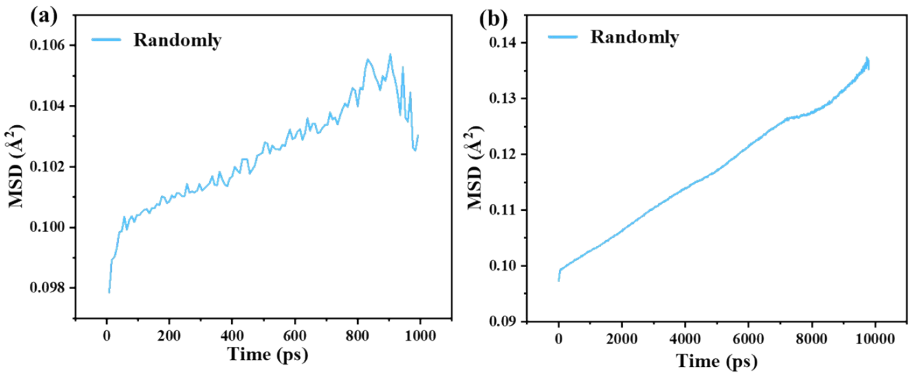

Fig. S7 The system with defects randomly distributes: (a) MSD curve of Li at 300 K with DPMD simulations of 1.2 ns. (b) MSD curve of Li at 300 K with DPMD simulations of 10.2 ns.